Transcriptomic Landscape of Prurigo Nodularis Lesional Skin CD3+ T Cells Using Single-Cell RNA Sequencing

Andreea Calugareanu, Florian Specque, Sarah Demouche, Chloé Grolleau, Gabor Dobos, Marine Merandet, David Bergerat, Sandy Peltier, Marie Jachiet, Charles Cassius, et al.

Transcriptomic Landscape of Prurigo Nodularis Lesional Skin CD3+ T Cells Using Single-Cell RNA Sequencing

Journal of Investigative Dermatology (2023) **143,** 2525–2529; doi:10.1016/j.jid.2023.05.011

TO THE EDITOR

Prurigo nodularis (PN) is a chronic inflammatory skin disease characterized by symmetrically distributed, widespread, pruritic nodules occurring in patients with chronic pruritus and may be associated with a history of atopic dermatitis (AD) (Pereira et al., 2018). The lack of approved therapies and the limited efficacy of off-label treatments reflect the poor understanding of PN pathogenesis (Williams et al., 2020). Previous studies have suggested roles for neuronal dysregulation, aberrant keratinocyte signaling, and underlying immune activation (Fukushi et al., 2011; Haas et al., 2010; Wong et al., 2020). Targeted real-time RT-qPCR, immunohistochemical staining, RNA sequencing, and clinical studies have suggested that PN has variable amounts of T helper (Th) 2, Th17, or Th22 signaling (Belzberg et al., 2021; Calugareanu et al., 2020; Fukushi et al., 2011; Park et al., 2011; Tsoi et al., 2022; Wong et al., 2020).

In this study, we performed single-cell RNA sequencing to comprehensively characterize the phenotypic variation of CD3$^+$ T cells and assess cell-specific gene expression in lesional skin from patients with PN (n = 6) versus from patients with AD (n = 5) and healthy controls (HCs) (n = 5). The results were confirmed using real-time qPCR and immunohistochemistry staining.

The study was reviewed and approved by the local ethics committee at Comite De Protection Des Personnes Ile De France IV (Paris, France), with written informed consent obtained from all patients. For patients' clinical characteristics, see Supplementary Table S1. CD3$^+$ T cells were sorted by flow cytometry from cell suspension obtained after enzymatic dissociation of skin samples and were subjected to droplet-based encapsulation (10x Genomics, Pleasanton, CA) followed by library preparation and sequencing as previously described. For extended methods, please see the Supplementary Materials and Methods.

A total of 12,964 cells (5,106 from patients with PN, 3,456 from those with AD, and 4,402 from HCs) that met the quality control metrics were aggregated and clustered into 12 distinct subsets according to their expression profiles by Uniform Manifold Approximation and Projection for dimension reduction (Figure 1a and Supplementary Figure S1 and Supplementary Table S2).

Among these clusters, three shared the expression of *CD4*, namely, CD4$^+$ T cells with a Th2/Th22 phenotype, regulatory CD4$^+$ T cells, and CD4$^+$ T cells with a Th17 polarization state (Figure 1b and c and Supplementary Figure S1). CD4$^+$ Th2/Th22 T cells were located in cluster 2, which was distinguished by abundant expression of types 2 and 22 associated genes *IL13*, *IL22,* and *IL4R* but also by upregulated expression of AD-associated cytokine *CSF2* (Choy et al., 2012). CD4$^+$ regulatory T cells were identified in cluster 3 by expression of signatures genes *FOXP3* and *IL2RA* and coinhibitory receptors *TIGIT* and *CTLA4*. CD4$^+$ T cells highly expressing markers associated with Th17, such as *KLRB1/CD161*, *CCL20,* and *RORA*, were present in cluster 6 (Reynolds et al., 2021; Rojahn et al., 2020). This cluster might thus be best described as containing CD4$^+$ Th17-polarized T cells despite a low percentage of cells highly expressing *IL17A* and *IL17F* cytokines.

Three clusters expressed *CD8A* and *CD8B* genes and exhibited distinct functional phenotypes (Figure 1b and c and Supplementary Figure S1): (i) CD8$^+$ T effector memory characterized by high expression of the NK-associated molecule *NKG7* (CD8$^+$ NK-like T cells) as well as other genes associated with cytotoxicity (*KLRG1*, *GZMK*, and *CCL4*), and IFN-associated genes (*IFNG* and *IFI16*) were found in cluster 5; (ii) high expression of genes encoding cytolytic enzymes (*GZMA* and *GZMB*) was found in cluster 8, but the high expression of genes associated with skin tissue residency (*CD69*, *RGS1*, and *NR4A1*) in this cluster suggested that it may represent a potential CD8+ cytotoxic tissue-resident memory T cell subset; and (iii) CD8+ tissue-resident memory T cells were located in cluster 9 and expressed both NK cell markers, such as *GNLY* and *KLRD1* (killer-like R family) as well as genes associated with skin tissue residency.

The remaining clusters showed none or random expression of *CD3*, *CD4,* or *CD8*. High expression of heat shock protein genes and *GADD45B* was identified in cluster 0. We therefore concluded that this cluster represents exhausted T cells. Cluster 7 was characterized by abundant expression of *KLF2*, a transcription factor expressed in single-positive CD4$^+$ and CD8$^+$ involved in T-cell homeostasis by mediating quiescence and survival (Jha and Das, 2017). We therefore described cluster 7 as containing quiescent memory T cells.

We determined the relative proportion of each cell type in all samples (Supplementary Figure S2a). Clusters 0, 4, and 8 contained substantial numbers of CD3$^+$ T cells from all patients with PN and AD and HCs. Nonetheless, we also observed clusters that were specific to either PN or AD (Supplementary Figure S2b). CD4+ Th2/Th22 and CD4+ regulatory T cell clusters consisted mostly of cells from AD (87 and 51%, respectively), whereas CD8+ NK-like T cells, CD4$^+$ Th17-polarized T

Abbreviation: AD, atopic dermatitis; HC, healthy control; PN, prurigo nodularis; Th, T helper

Accepted manuscript published online 30 May 2023; corrected proof published online 5 July 2023

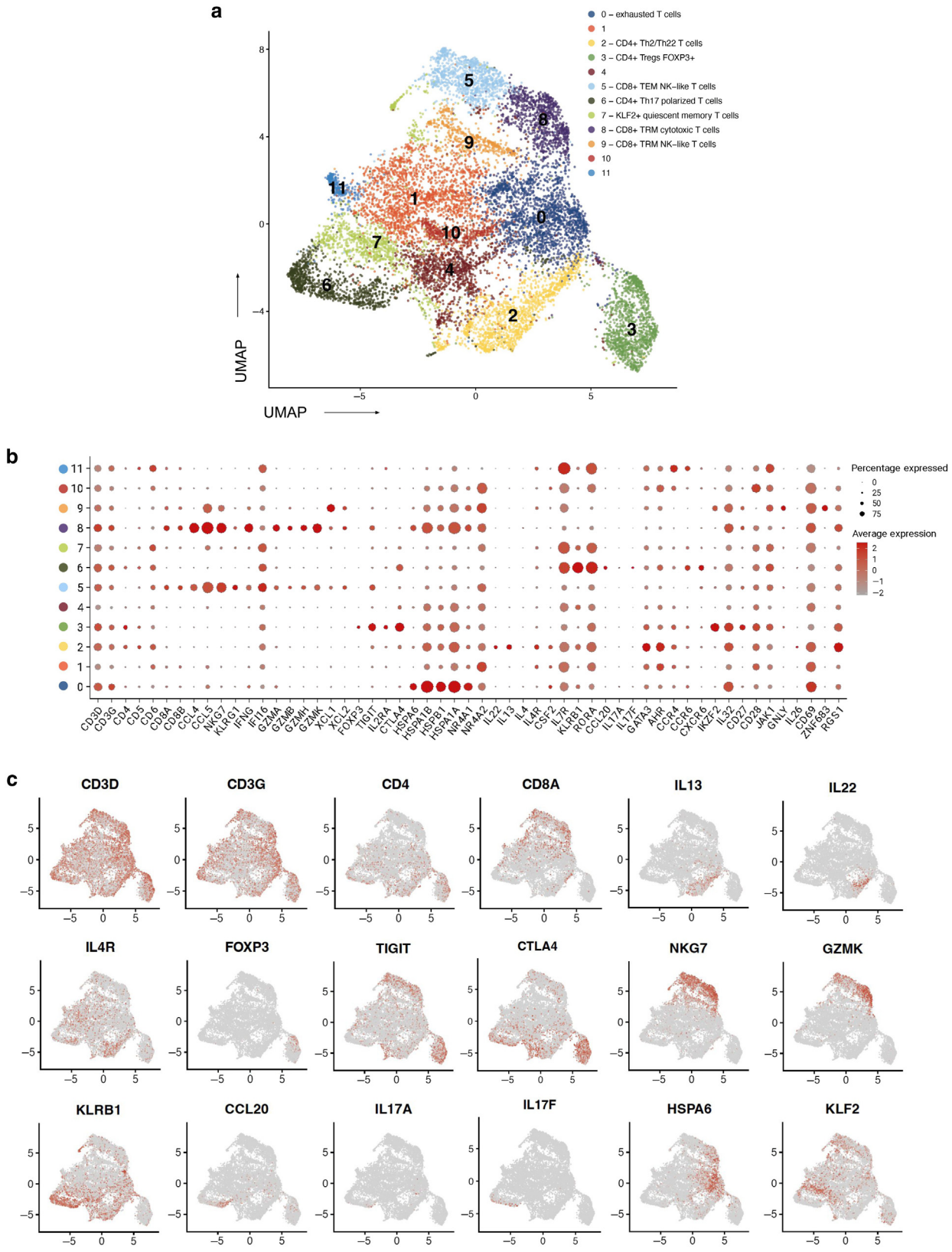

Figure 1. Transcriptional profiles of CD3$^+$ T lymphocytes from the skin samples of patients with PN and AD and HCs analyzed by scRNA-seq. (**a**) UMAP plot for 12,964 skin CD3+ T lymphocytes (5,106 cells derived from six patients with PN, 3,456 cells derived from five patients with AD, and 4,402 cells derived from five HCs) revealed 12 Louvain clusters. (**b, c**) Feature plots of expression distribution for cluster-specific marker genes. Expression levels for each cell are color coded and overlaid onto UMAP plots. Red color intensity represents a respective level of expression. AD, atopic dermatitis; HC, healthy control; PN, prurigo nodularis; scRNA-seq, single-cell RNA sequencing; TEM, effector memory T cell; Th, T helper; Treg, regulatory T cell; TRM, tissue-resident memory; UMAP, Uniform Manifold Approximation and Projection.

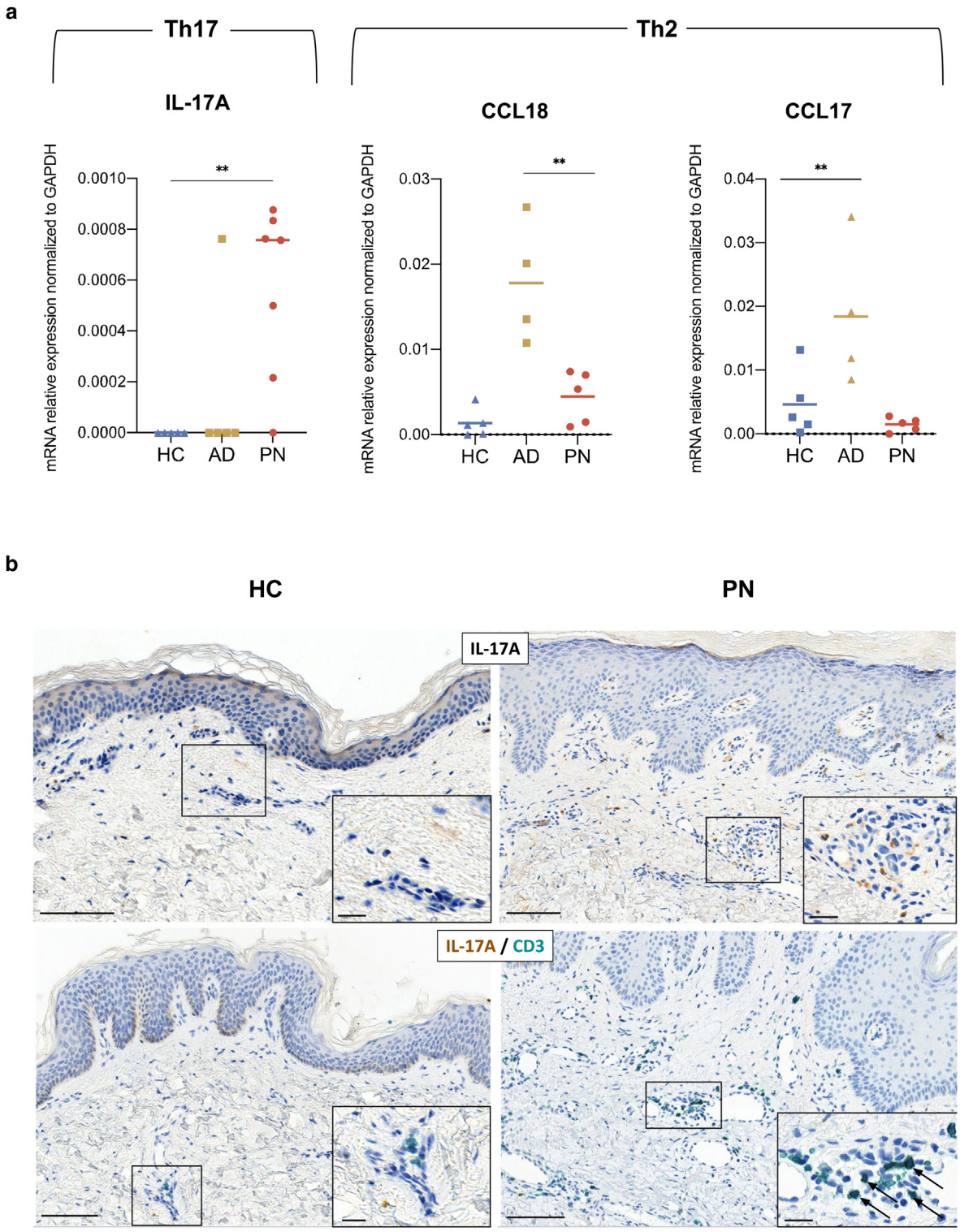

Figure 2. Real-time qPCR and IHC testing and real-time qPCR in patients with PN and AD and HCs. (**a**) Bar graph showing mRNA expression of Th17-associated *IL17A* cytokine and Th2-related genes *CCL17* and *CCL18* in archival lesional skin samples from patients with PN (n = 6), patients with AD (n = 4), and HCs (n = 5). Analysis was performed with Student *t*-test. *$P < 0.05$, **$P < 0.01$, and ***$P < 0.001$. (**b**) IL-17A and CD3 IHC staining of skin biopsies from HCs (left panels, at ×15; inset in panels are at ×40) and patients with PN (right panels, ×15; inset in panels are at ×40). Bar = 100 μm for panels at ×15 and 20 μm for panels at ×40. Arrows indicate some of the cells expressing both IL-17A and CD3. AD, atopic dermatitis; HC, healthy control; IHC, immunohistochemistry; PN, prurigo nodularis; Th, T helper.

cells, and KLF2+ quiescent memory T cells clusters consisted mostly of cells from patients with PN (54, 88, and >80%, respectively). Interestingly, CD4$^+$ Th17-polarized T cells (cluster 6) predominantly originated from patients with PN (87.9% compared with 7.5% and 4.6% from HCs and patients with AD, respectively), supporting a pathogenic role for the Th17 pathway within the lesional skin of patients with PN. Furthermore, Th17-associated

IL17A and *IL17F* gene cytokines were found to be significantly expressed in PN samples compared with those in AD samples and samples from HC ($P < 0.0001$) (Supplementary Figure S2c). Previous studies have also revealed variable amounts of Th17 signaling in PN (Belzberg et al., 2021; Wong et al., 2020).

We then performed RT-qPCR to analyze the mRNA expression of Th17-associated *IL17A* cytokine and Th2-related genes *CCL17* and *CCL18* in lesional skin samples from patients with PN (n = 6), patients with AD (n = 4), and HCs (n = 5). Skin samples from patients with PN showed significantly higher expression of *IL17A* ($P < 0.01$) than those from patients with AD and the HCs (Figure 2a). Furthermore, we performed immunohistochemistry staining for CD3 and IL17A in five randomly selected cases of PN and HC each. Immunohistochemistry staining was positive for IL17A in skin samples from patients with PN. The vast majority of IL-17A−positive cells also colabeled with CD3, suggesting that they may represent type 17−polarized T cells (Figure 2b). In comparison, no IL-17A signal was detected in biopsies obtained from HCs.

This study has some limitations because it involves a limited number of samples, restricting our ability to better resolve some T cell subsets. Another limitation of the study is that age and body sites show some bias. This is due to the incidence and prevalence of both of these skin conditions.

In conclusion, we present in this study, to our knowledge, a previously unreported single-cell transcriptomic analysis of CD3$^+$ T cells isolated from skin biopsy samples from patients with PN. Our results confirm the molecular heterogeneity of PN and suggest that it may be driven by more heterogeneous CD3$^+$ T cell subsets than previously thought. Understanding the biology of these cells and their biomarkers may lead to future potential areas of investigation for precision medicine in PN therapeutic management.

Data availability statement

All data referenced in this study are included in the figures, tables, and Supplementary Materials and Methods. Raw and processed single-cell RNA-sequencing data for all samples have been deposited in the Gene Expression Omnibus database under access code GSE213849 (https://www.ncbi.nlm.nih.gov/geo/query/acc.cgi?acc=213849).

ORCIDs

Andreea Calugareanu: http://orcid.org/0000-0003-2841-1680
Florian Specque: http://orcid.org/0000-0002-4449-6381
Sarah Demouche: http://orcid.org/0000-0001-7751-6011
Chloe Grolleau: http://orcid.org/0000-0002-8393-7442
Gabor Dobos: http://orcid.org/0000-0002-2544-7197
Marine Merandet: http://orcid.org/0000-0001-8397-8677
David Bergerat: http://orcid.org/0000-0003-0013-6621
Sandy Peltier: http://orcid.org/0000-0002-5520-7346
Charles Cassius: http://orcid.org/0000-0002-5087-4414
Marie Jachiet: http://orcid.org/0000-0001-5286-9689
Thibault Mahevas: http://orcid.org/0000-0001-5951-1831
Anne Saussine: http://orcid.org/0000-0002-2419-4677
Alexandre How-Kit: http://orcid.org/0000-0002-1584-9336
Rachel Onifarasoaniaina: http://orcid.org/0000-0002-0355-1882
Kevin Serror: http://orcid.org/0000-0002-2517-1039
Mylène Bohec: http://orcid.org/0000-0002-6530-596X
Sylvain Baulande: http://orcid.org/0000-0003-3104-1684
Clemence Lepelletier: http://orcid.org/0000-0003-3204-9194
Marc Mrad: http://orcid.org/0000-0001-8423-6122
Estelle Charvet: http://orcid.org/0000-0003-1841-3471
Adèle de Masson: http://orcid.org/0000-0001-7828-6211
David Boccara: http://orcid.org/0000-0002-7365-5943
Maxime Battistella: http://orcid.org/0000-0002-7053-7431
Hélène Le Buanec: http://orcid.org/0000-0002-2139-0357
Jean-David Bouaziz: http://orcid.org/0000-0002-4993-2461

CONFLICT OF INTEREST

MJ and JDB are speakers, scientific advisers, consultants, and/or clinical study investigators for Sanofi Genzyme. JDB is a speaker, scientific adviser, consultant, and/or clinical study investigator for Galderma. The remaining authors state no conflict of interest.

ACKNOWLEDGMENT

This work was supported by Sanofi Genzyme Type 2 Innovation Grant and in part by a grant from the Société Française de Dermatologie. The authors thank Remulus Catana for his valuable advice on data analysis.

AUTHOR CONTRIBUTIONS

Conceptualization: AC, GD, HLB, JDB; Data Curation: AC, FS, GD, HLB, JDB, SB, MB; Formal Analysis: AC, FS, HLB, MB; Funding Acquisition: AC, JDB; Investigation: AC, GD, SD, CG, MM, DB, SP, MB, HLB; Methodology: AC, FC, HLB, JDB; Project Administration: JDB, HLB; Resources: AC, GD, HLB, JDB, CC, TM, AS, KS, DB, MB, CL, MM, EC, ADM; Software: AC, FS, HLB; Supervision: AC, HLB, JDB; Validation: AC, FS, SD, CG, GD, MM, DB, CG AHK, RO; Visualization: AC, FS, SD, CG, MM, DB, MB, RO, MB, HLB, JDB; Writing - Original Draft Preparation: AC, FC, HLB; Writing - Review and Editing: AC, FS, SD, CG, GD, MM, DB, SP, MJ, CC, TM, AS, AHK, MB, SB, CL, MM, EC, RO, ADM, DB, MB, HLB, JDB

***Andreea Calugareanu*[1,2], *Florian Specque*[3], *Sarah Demouche*[1,2], *Chloe Grolleau*[1,2], *Gabor Dobos*[4], *Marine Merandet*[1], *David Bergerat*[1], *Sandy Peltier*[1], *Marie Jachiet*[2], *Charles Cassius*[1,2], *Thibault Mahevas*[2], *Anne Saussine*[2], *Alexandre How-Kit*[5], *Rachel Onifarasoaniaina*[6], *Kevin Serror*[1,7], *Mylène Bohec*[8], *Sylvain Baulande*[8], *Clemence Lepelletier*[2], *Marc Mrad*[2], *Estelle Charvet*[2], *Adèle de Masson*[1,2,9], *David Boccara*[1,6,9], *Maxime Battistella*[1,9,10], *Hélène Le Buanec*[1,11] and *Jean-David Bouaziz*[1,2,9,*,11]**

[1]INSERM U976, Hôpital Saint-Louis, Paris, France; [2]Dermatology Department, Hôpital Saint-Louis, Assistance Publique-Hôpitaux de Paris, Paris, France; [3]Clinical Research and Bioinformatics Unit, Hôpital Saint-Louis, Assistance Publique-Hôpitaux de Paris, Paris, France; [4]Skin Tumor Centre Charité (HTCC), Department of Dermatology, Venereology and Allergology, Charité-Universitätsmedizin Berlin, Berlin, Germany; [5]Laboratory of Genomics, Foundation Jean Dausset-CEPH, Paris, France; [6]Institut Cochin, INSERM U1016, CNRS UMR8104, Université de Paris, Paris, France; [7]Department of Plastic Surgery and Burn Unit, Hôpital Saint-Louis, Assistance Publique-Hôpitaux de Paris, Paris, France; [8]Institut Curie Genomics of Excellence (ICGex) Platform, Paris, France; [9]Université de Paris, Paris, France; and [10]Pathology department, Hôpital Saint-Louis, Assistance Publique-Hôpitaux de Paris, Paris, France

[11]These authors contributed equally to this work.

[*]Corresponding author. e-mail: jean-david.bouaziz@aphp.fr

SUPPLEMENTARY MATERIAL

Supplementary material is linked to the online version of the paper at www.jidonline.org, and at https://doi.org/10.1016/j.jid.2023.05.011.

REFERENCES

Belzberg M, Alphonse MP, Brown I, Williams KA, Khanna R, Ho B, et al. Prurigo nodularis is characterized by systemic and cutaneous T

helper 22 immune polarization. J Invest Dermatol 2021;141:2208–18.e14.

Calugareanu A, Jachiet M, Tauber M, Nosbaum A, Aubin F, Misery L, et al. Effectiveness and safety of dupilumab for the treatment of prurigo nodularis in a French multicenter adult cohort of 16 patients. J Eur Acad Dermatol Venereol 2020;34:e74–6.

Choy DF, Hsu DK, Seshasayee D, Fung MAMZ, Martin F, et al. Comparative transcriptomic analyses of atopic dermatitis and psoriasis reveal shared neutrophilic inflammation. J Allergy Clin Immunol 2012;130:1335–43.e5.

Fukushi S, Yamasaki K, Aiba S. Nuclear localization of activated STAT6 and STAT3 in epidermis of prurigo nodularis. Br J Dermatol 2011;165:990–6.

Haas S, Capellino S, Phan NQ, Böhm M, Luger TA, Straub RH, et al. Low density of sympathetic nerve fibers relative to substance P-positive nerve fibers in lesional skin of chronic pruritus and prurigo nodularis. J Dermatol Sci 2010;58:193–7.

Jha P, Das H. KLF2 in regulation of NF-κB-mediated immune cell function and inflammation. Int J Mol Sci 2017;18:2383.

Park K, Mori T, Nakamura M, Tokura Y. Increased expression of mRNAs for IL-4, IL-17, IL-22 and IL-31 in skin lesions of subacute and chronic forms of prurigo. Eur J Dermatol 2011;21:135–6.

Pereira MP, Steinke S, Zeidler C, Forner C, Riepe C, Augustin M, et al. European academy of dermatology and venereology European prurigo project: expert consensus on the definition, classification and terminology of chronic prurigo. J Eur Acad Dermatol Venereol 2018;32:1059–65.

Reynolds G, Vegh P, Fletcher J, Poyner EFM, Stephenson E, Goh I, et al. Developmental cell programs are co-opted in inflammatory skin disease. Science 2021;371:eaba6500.

Rojahn TB, Vorstandlechner V, Krausgruber T, Bauer WM, Alkon N, Bangert C, et al. Single-cell transcriptomics combined with interstitial fluid proteomics defines cell type-specific immune regulation in atopic dermatitis. J Allergy Clin Immunol 2020;146:1056–69.

Tsoi LC, Hacini-Rachinel F, Fogel P, Rousseau F, Xing X, Patrick MT, et al. Transcriptomic characterization of prurigo nodularis and the therapeutic response to nemolizumab. J Allergy Clin Immunol 2022;149:1329–39.

Williams KA, Huang AH, Belzberg M, Kwatra SG. Prurigo nodularis: pathogenesis and management. J Am Acad Dermatol 2020;83:1567–75.

Wong LS, Yen YT, Lin SH, Lee CH. IL-17A induces endothelin-1 expression through p38 pathway in prurigo nodularis. J Invest Dermatol 2020;140:702–6.e2.

Itch Is More Important than Clinical Disease Severity for Depression in Psoriasis: A Prospective Register Study

JID Open

Journal of Investigative Dermatology (2023) **143,** 2529–2532; doi:10.1016/j.jid.2023.05.007

TO THE EDITOR

Psoriasis is associated with depression, but the reasons for this are not fully understood (Kleyn et al., 2020). It is believed that the severity of the skin disease, itch intensity, and systemic inflammation are important associated factors (Farzanfar et al., 2018; Reich et al., 2016a; Tee et al., 2016). To better understand the extent to which skin disease severity and itch contribute to depression in patients with psoriasis, we conducted a real-world registry study on the DermaReg register.

DermaReg enrolls patients treated with systemics for psoriasis in Stockholm, Sweden and prospectively conducts follow-ups (Svedbom et al., 2020; Svedbom and Ståhle, 2020). The study was approved by the Swedish Ethical Review Authority. All patients gave written informed consent to participate in DermaReg.

The main outcome in this study was depressive symptoms measured using the Montgomery–Åsberg Depression Rating Scale - Self Assessment (MADRS-S) (Svanborg and Asberg, 1994). MADRS-S covers nine domains, and the total score ranges from 0 to 54. We categorized the scores into no (0–12), mild (13–19), moderate (20–34), and severe (≥35) depression. In sensitivity analysis, we used the anxiety/depression dimension from the EuroQol 5-Dimension 3-Level (EQ-5D-3L) instrument (Oppe et al., 2007) as an outcome. Respondents to the EQ-5D-3L anxiety/depression dimension chose one of three levels for the level of anxiety/depression, and we categorized these as mo, moderate, and severe depression.

The exposures were measured in terms of psoriasis disease severity using PASI (Fredriksson and Pettersson, 1978), and average itch during the last 3 days was measured using a Visual Analog Scale (VAS), ranging from 0 to 10 (Reich et al., 2016b).

We included the following confounders: sex, age, current smoking, risky use of alcohol, and body mass index. Covariates were obtained as close as possible to the visit with exposure and outcome data.

In terms of mediators, we investigated the mediating effect of the Dermatology Life Quality Index (DLQI) (Finlay and Khan, 1994) on the associations between PASI and itch VAS and MADRS-S. Should the association between MADRS-S and the exposures be fully mediated by the DLQI, assessing the DLQI may be sufficient to measure the impact of signs and symptoms of psoriasis on depression. We included all observations with full data on exposures and outcomes in the analysis. We described the crude associations between exposure and outcomes by estimating the prevalence of depression by deciles for each exposure. We also estimated the Pearson correlation between the exposures and outcomes.

To estimate and compare the impact of itch VAS and PASI on depression, we centered and scaled PASI and itch VAS by their respective means and SDs. We estimated the associations between mean-standardized exposures and mild, moderate, and severe depression

Abbreviations: CI, confidence interval; DLQI, Dermatology Life Quality Index; EQ-5D-3L, EuroQol 5-Dimension 3-Level; MADRS-S, Montgomery–Åsberg Depression Rating Scale – Self Assessment; VAS, Visual Analog Scale

Accepted manuscript published online 29 May 2023; corrected proof published online 8 July 2023

SUPPLEMENTARY MATERIALS AND METHODS

Patients and samples information

The study was reviewed and approved by the local ethics committee at Comite De Protection Des Personnes Ile De France IV (Paris, France) (reference 220 B19), with written informed consent on the use of skin biopsies for research purposes obtained from all patients, according to French ethical rules. Patients and their baseline clinical characteristics are depicted in Supplementary Table S1. Patients with clinical diagnoses of moderate-to-severe prurigo nodularis (n = 6) and atopic dermatitis (n = 5) and histologic confirmation were recruited from the Dermatology Department of Saint Louis Hospital (Paris, France). Patients with prurigo nodularis and atopic dermatitis had no topical steroid/immunomodulator use in the last 2 weeks, no systemic immunosuppressants or phototherapy in the last 12 weeks, and no moisturizer use within 12 hours. Two 4-mm punch skin biopsies were obtained from lesional skin after a washout period of topical treatments (2 weeks) and systemic treatments (3 months). Regarding patients with prurigo nodularis, biopsy specimens were taken from recently developed dome-shaped, erythematous, and pruriginous nodules without excoriated/ulcerated areas. A skin sample was placed in formalin and embedded in paraffin for histopathologic evaluation. The other skin sample was stored in MACS Tissue Storage Solution (Miltenyi Biotec, Bergisch Gladbach, Germany) and kept for 3−4 hours at 4 °C until further processing. Healthy control samples were obtained from the discarded skin of healthy individuals undergoing plastic surgery (4-mm punch skin biopsies).

Preparation of cell suspension and isolation of lymphocytes from human skin using flow cytometry

Isolation of whole lymphocytes from the skin samples was performed as previously described (Miragaia et al., 2019). In brief, skin samples underwent excision of the hypoderm, and the dermoepidermal part was incubated overnight together with enzyme P, enzyme D, and enzyme A from the Whole Skin Dissociation kit (Miltenyi Biotec) for 11−12 hours at 37 °C and 5% carbon dioxide. Mechanical dissociation was then performed using the gentleMACS Dissociator (Miltenyi Biotec, Bergisch Gladbach, Germany) according to the manufacturer's instructions. Cell suspensions were sorted for CD3+ T cells using flow cytometry on the basis of differences in forward scatter and side scatter distribution after immunostaining with anti-CD3+ mAbs (Miltenyi Biotec, Bergisch Gladbach, Germany). Cells viability was assessed using fixable viability dyes for flow cytometry (Fixable Viability Stain 510, BD Biosciences, Franklin Lakes, NJ) as well as using Trypan blue (1450013, Bio-Rad Laboratories, Hercules, CA) exclusion method on a Countess automated cell counter (Invitrogen, Waltham, MA). Samples with >90% viability after lymphocyte extraction were used for further single-cell RNA-sequencing analysis.

Single-cell capture, droplet-based single-cell RNA-sequencing analysis, and data processing

Single cells were captured using the droplet-based microfluidic Chromium Controller system (10x Genomics, Pleasanton, CA) according to the manufacturer's instructions. Lymphocyte concentrations were adjusted to load 2,000 cells and enable the capture of ∼1,000 cells per tissue sample. Cell suspensions were loaded onto separate chip inlets to perform cell encapsulation into droplets. Reverse transcription, cDNA generation, and library preparation were achieved using the standard 10x Genomics single-cell protocol (Chromium Single Cell 3′ Reagent Kit, version 3.1). Libraries were sequenced on the Illumina NovaSeq6000 platform (Illumina, San Diego, CA) following the manufacturer's instructions to obtain ∼50 million reads per sample.

Clustering analysis using Seurat and Uniform Manifold Approximation and Projection visualization

Raw-sequencing data were demultiplexed, aligned to a reference genome (GrCh38), and counted using Cell Ranger (version 3.0.2, 10x Genomics). The secondary analysis was carried out using R (version 4.1.3, available from https://www.r-project.org) and the Seurat package (version 4.0.3, Satija Lab, New York University, New York, NY) according to the recommended protocol (Satija et al., 2015). Cells with fewer than 150 genes or more than 20% mitochondrial gene content were excluded. Genes with less than 20 counts across the whole dataset were also discarded. Standard Seurat protocol was then performed; counts were log normalized and scaled before principal component analysis to compute 100 principal components on the basis of 2,000 most variable features detected by vst. A total of 65 first principal components were used as input for clustering analysis by the Louvain algorithm with multilevel refinement (30 nearest neighbors with the cosine metric and a resolution of 0.8 [Becht et al., 2018; Macosko et al., 2015]). A Uniform Manifold Approximation and Projection was computed, and cells were colorized according to their cluster. Differential gene expression analysis was fulfilled with the Wilcoxon rank-sum test with Bonferroni correction for adjusted *P*-values of 0.05 or less. Cell types within clusters were manually determined on the basis of their top differentially expressed genes. Raw and processed single-cell RNA-sequencing data for all samples have been deposited in the Gene Expression Omnibus database under access code GSE213849 (https://www.ncbi.nlm.nih.gov/geo/query/acc.cgi?acc=213849). Subsequent statistical analysis was carried out on R 4.1.3 using the Wilcoxon rank-sum test, and *P*-values were adjusted with the Benjamini−Hochberg procedure.

Real-time qPCR

Real-time qPCR was carried out using the LightCycler 480 SYBR Green I Master (Roche, Basel, Switzerland) after reverse transcription from 56 ng total RNA (SuperScript IV VILO Master Mix with ezDase Enzyme, Thermo Fisher Scientific, Waltham, MA). All primers were purchased from TIB Molbiol (Berlin, Germany) and were as followed (listed 5′->3′): TGCACCACCAACTG CTTAGC (forward) and GGCATGGAC TGTGGTCATGAG (reverse) for GAP DH, 5′-ACT ACA ACC GAT CCA CCT CAC-3′ (forward) and 5′-ACT TTG CCT CCC AGA TCA CAG-3′ (reverse) for

IL-17A, CTGCTGACGATGATGAAGG AGAAC (forward) and TTGTCACA GGCACTAAGGAAGTT (reverse) for S100A7, GCTGGAACGCAACATAGA-GAC (forward) and TCACAGAGT ATTGGTGGAAGG-T (reverse) for S100A9, TCCAGGGACGAAGAAGAG (forward) and GGCTCCAGTTCAGACA AG (reverse) for CCL17, and CGGAAT CACAGACTGAGAGGAATT (forward) and CTTGCTGTTTCTGCCCCTTTTC (reverse) for CCL18.

PCR conditions were 95 °C for 5 minutes, followed by 60 cycles of 95 °C for 10 seconds, 60 °C for 20 seconds, and 72 °C for 5 minutes. *GAPDH* was used as the reference gene for normalization. The relative expression levels of mRNA were determined using the dCT formula, and fold changes were calculated as 2^-dCT.

Immunohistochemistry

Immunostaining was performed at the Cochin HistIM Facility (Paris, France). For immunochemistry, slides were performed on the automaton Leica Bond RX. Slides were incubated for 15 minutes at 95 °C in a solution of deparaffinization and antigen retrieval at pH 6. Then, they were rinsed and incubated for 20 minutes at room temperature with anti−IL-17A antibody (AF-317-SP, R&D Systems, Minneapolis, MN) at 1/100 and anti-CD3 antibody (MA1-90582, Invitrogen, Waltham, MA) at 1/100. The revelation in brightfield was performed by Bond Intense R Detection (DS 9263, Leica, Wetzlar, Germany). Sections were lightly counterstained with hematoxylin, then dehydrated and cleared in graded alcohol and Ottix plus (MM-France, Paris, France), and finally covered with glass slips.

SUPPLEMENTARY REFERENCES

Becht E, McInnes L, Healy J, Dutertre CA, Kwok IWH, Ng LG, et al. Dimensionality reduction for visualizing single-cell data using UMAP. Nat Biotechnol 2018.

Macosko EZ, Basu A, Satija R, Nemesh J, Shekhar K, Goldman M, et al. Highly parallel genome-wide expression profiling of individual cells using nanoliter droplets. Cell 2015;161:1202−14.

Miragaia RJ, Gomes T, Chomka A, Jardine L, Riedel A, Hegazy AN, et al. Single-cell transcriptomics of regulatory T cells reveals trajectories of tissue adaptation. Immunity 2019;50:493−504.e7.

Satija R, Farrell JA, Gennert D, Schier AF, Regev A. Spatial reconstruction of single-cell gene expression data. Nat Biotechnol 2015;33:495−502.

Supplementary Figure S1. Transcriptional profiles of CD3$^+$ T lymphocytes from the skin samples of patients with PN and AD and HCs analyzed by scRNA-seq. Distinct gene signatures (top 10 differentially expressed genes; Wilcoxon rank-sum test) of CD3$^+$ lymphocytes T-cell subsets are shown. AD, atopic dermatitis; HC, healthy control; PN, prurigo nodularis; scRNA-seq, single-cell RNA sequencing.

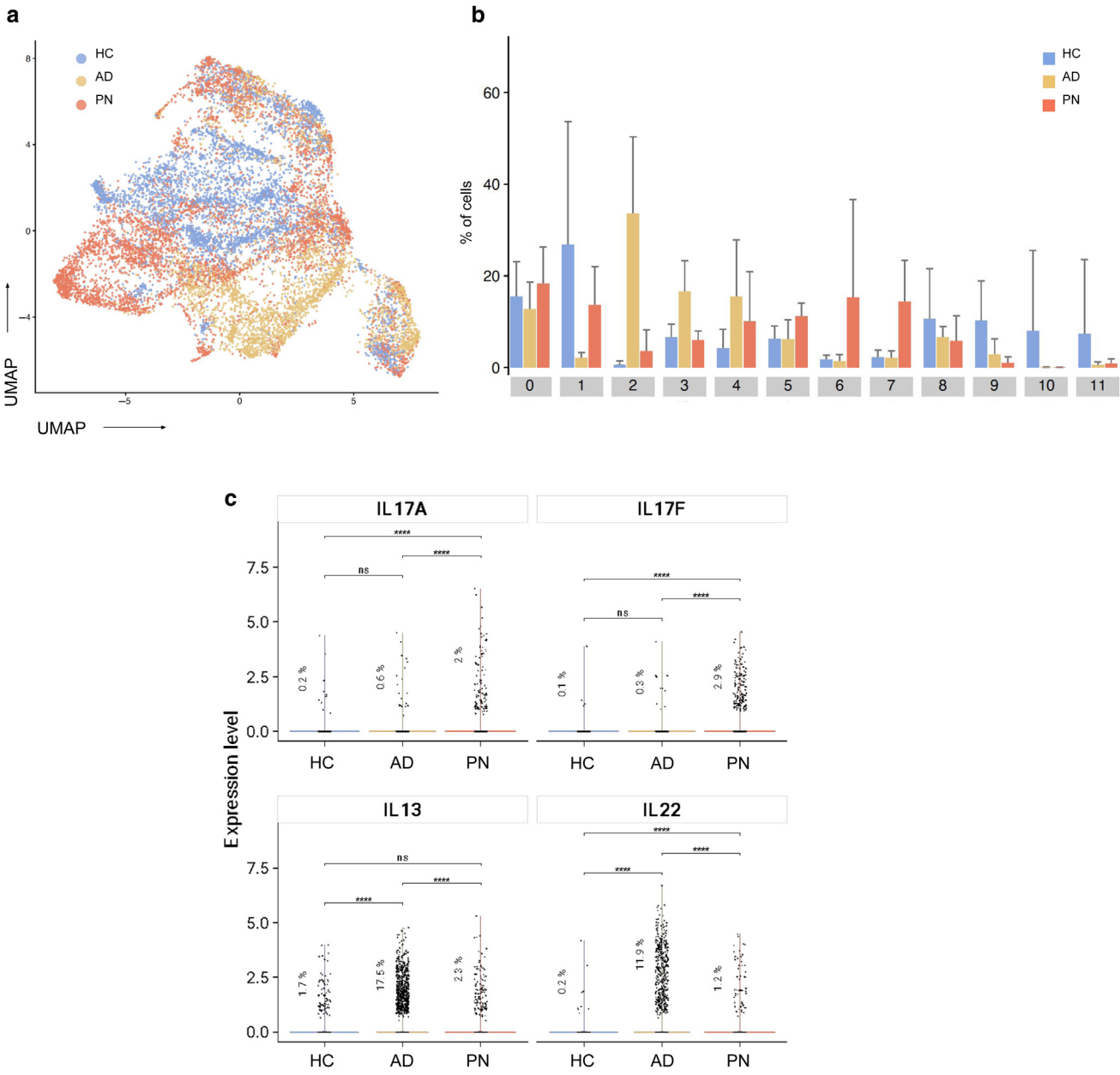

Supplementary Figure S2. Heterogeneity of CD3$^+$ T cells in prurigo nodularis, atopic dermatitis, and healthy skin. (**a**) UMAPs showing 12,964 CD3$^+$ T lymphocytes colored by condition. (**b**) Proportions of cluster-originating CD3$^+$ T cells per patient (referred to as the cluster weights per patient). Colored bars represent the mean of cluster weights for all patients, distributed according to their clinical status. Error bars depict the SD from the mean. (**c**) Expression level of IL-17A, IL-17F, IL-13, and IL-22 in healthy participants and participants with atopic dermatitis and prurigo nodularis. Statistical tests are unadjusted; analysis was performed with Wilcoxon rank-sum tests. ****$P < 0.0001$. AD, atopic dermatitis; HC, healthy control; ns, nonsignificant; PN, prurigo nodularis; UMAP, Uniform Manifold Approximation and Projection.

Supplementary Table S1. Sample Description

Sample	Sex	Age	Race	Condition	Atopic Predisposition	Peak Itch NRS	Disease Activity (IGA)	Sample Site
HC_01	F	60	White	HC	N/A	N/A	N/A	Upper left arm
HC_02	F	27	White	HC	N/A	N/A	N/A	Breast
HC_03	F	54	White	HC	N/A	N/A	N/A	Breast
HC_04	M	32	White	HC	N/A	N/A	N/A	Upper left arm
HC_05	F	36	White	HC	N/A	N/A	N/A	Breast
PN_01	M	78	White	PN	No	8	Severe	Upper left leg
PN_02	M	63	White	PN	No	10	Severe	Upper right arm
PN_03	F	49	AA	PN	Yes (AD)	9	Severe	Upper right leg
PN_04	F	43	White	PN	No	8	Severe	Upper right arm
PN_05	M	55	White	PN	No	9	Moderate	Upper left leg
PN_06	F	52	AA	PN	No	7	Severe	Lower right arm
AD_01	M	26	White	AD	Yes	7	Severe	Anterior thorax
AD_02	F	18	White	AD	Yes	10	Moderate	Upper right arm
AD_03	F	30	White	AD	Yes	9	Severe	Upper right leg
AD_04	M	54	White	AD	Yes	8	Severe	Anterior thorax
AD_05	M	20	White	AD	Yes	8	Moderate	Upper right leg

Abbreviations: AA, African American; AD, atopic dermatitis; F, female; HC, healthy control; IGA, Investigator Global Assessment; M, male; NRS, numeric rating scale; N/A, not applicable; PN, prurigo nodularis.

Clinical features collected for each patient/sample used in the single-cell RNA-sequencing analysis are shown. IGA score of disease activity ranged from 0 (clear) to 4 (severe). NRS (last 24 hours) ranged from 0 (none) to 10 (severe).